Comparative Analysis of Various Interaction Effects for Piled Rafts in Sands Using Centrifuge Tests

Dongyu Park[1] and Junhwan Lee[2]

Abstract: In the current study, the load responses and interaction effects of piled rafts embedded in sands were investigated. A series of centrifuge load tests were conducted using different types of model foundations. Single piles, group piles, piled rafts, and unpiled rafts were adopted in the tests to analyze various interaction effects of piled rafts. The load-settlement curves of piled rafts were similar to those of group piles for the initial settlement range and became similar to those of rafts as settlement increased. The pile-group, pile-to-raft, and raft-to-pile interaction factors showed state-dependent and nonlinear variations with settlement. Both pile-to-raft and raft-to-pile interaction factors decreased within the initial settlement range and increased with increasing settlement. The range of pile-to-raft interaction factor values was much larger than the range of values for the raft-to-pile interaction factor. The load response and load transfer relationship of piles for piled rafts were different from those of single piles, showing that the effect of raft-to-pile interaction was more dominant within the upper soil zone. The mobilized factor of safety for rafts was always higher than the safety factor of piles and piled rafts because of the lower mobilized load-carrying capacity of rafts. **DOI:** 10.1061/(ASCE)GT.1943-5606.0001183.

Author keywords: Piled rafts (PRs); Interaction effects; Sands; Settlement; Group piles (GPs); Factor of safety (FS); Unpiled rafts (URs).

Introduction

The piled rafts (PRs) were developed to use the load-carrying capacities of both rafts and piles as an optimized foundation type and design concept (Davis and Poulos 1972; Burland 1995). Because PRs represent a combined structural system of different foundation components, interaction effects arise and affect the overall load response of PRs (Long 1993; Horikoshi and Randolph 1996; Katzenbach et al. 2000). If a load imposed on a PR were assumed to be carried solely by piles without considering the load-carrying capacity of the raft, the design of the PR would become overly conservative. On the other hand, the design may not be conservative enough if the load-carrying capacities of rafts and piles are fully considered without clear identification of the interaction effects. As neither case is desired, the interaction effects of PRs need to be clarified and properly taken into account in foundation design.

The interactions of PRs occur because of the overlapped stress and displacement fields of rafts and piles, resulting in a complex load-carrying mechanism. The interaction effects of PRs can be categorized into (1) pile-to-pile (P-P); (2) raft-to-pile (R-P); and (3) pile-to-raft (P-R) (Katzenbach et al. 2000). The P-P interaction effect is also referred to as the pile group effect. The R-P and P-R interaction effects represent the interactive effects between rafts and piles, which produce different load responses from those of unpiled rafts (URs) and group piles (GPs) PRs. According to Long (1993), the R-P interaction effect can cause the load capacity of piles for PRs to be larger than the load capacity of GPs. Downward soil movement upon loading on rafts, on the other hand, may reduce pile skin friction because of decreasing relative displacement between piles and soils (Han and Ye 2006).

There have been extensive investigations on PR interaction effects (Liu et al. 1985; Long 1993; Horikoshi and Randolph 1998; Conte et al. 2003; Reul and Randolph 2003; de Sanctis and Mandolini 2006). Liu et al. (1985) conducted field load tests and suggested raft-pile-soil interaction factors based on the PR geometric configuration. Horikoshi and Randolph (1998) performed finite-element analysis and proposed an interaction factor as a function of raft and pile stiffness and of PR configuration parameters. Most previous investigations on PR interactions focused on the roles and effects of foundation configuration and property conditions. As different design settlements are specified in the performance-based foundation design, it is also important to address the settlement-dependent characteristics of interaction effects with individual and interactive load-carrying mechanisms of rafts and piles.

In the current study, the load response and effects of interactions for PRs embedded in sands are investigated considering different interaction components. For this purpose, various PR interaction effects reported in the literature were reviewed, and a series of centrifuge load tests were conducted using model foundations. The UPs and PRs and single piles (SPs) and GPs were prepared and adopted in the tests. The model foundations were instrumented to measure detailed load response and load transfer mechanisms. From the test results, key characteristics of interaction effects and interaction factors are presented and discussed.

Load-Carrying Mechanism and Interactions of PRs

Load-Carrying Capacity

The load capacity of PRs is composed of those of rafts and piles and can be expressed as follows:

[1]Ph.D. Candidate, School of Civil and Environmental Engineering, Yonsei Univ., 134 Shinchon-dong, Seodaemun-gu, Seoul 120-749, Korea.

[2]Professor, School of Civil and Environmental Engineering, Yonsei Univ., 134 Shinchon-dong, Seodaemun-gu, Seoul 120-749, Korea (corresponding author). E-mail: junlee@yonsei.ac.kr

Note. This manuscript was submitted on May 23, 2013; approved on August 20, 2014; published online on September 23, 2014. Discussion period open until February 23, 2015; separate discussions must be submitted for individual papers. This paper is part of the ***Journal of Geotechnical and Geoenvironmental Engineering***, © ASCE, ISSN 1090-0241/04014082 (10)/$25.00.

$$Q_{pr} = Q_r + Q_p \tag{1}$$

where Q_{pr} = load-carrying capacity of PR; and Q_r and Q_p = load-carrying capacities of raft and pile components. The mobilized stress and displacement fields of rafts and piles overlap within the soil, producing complex load-carrying mechanisms and different types of interaction effects. Q_r and Q_p in Eq. (1) differ from those of URs and GPs because of the interactions between rafts and piles when combined into a PR.

Fig. 1 shows the schematic view of PR interactions that are categorized into (1) P-P; (2) R-P; and (3) P-R interactions (Katzenbach et al. 2000). Considering the interaction effects in Fig. 1, Eq. (1) can be rewritten in terms of the load capacities of URs and GPs as follows:

$$Q_{pr} = \eta_r \cdot Q_{ur} + \eta_p \cdot Q_{gp} = \eta_r \cdot Q_{ur} + \eta_p \cdot \chi_g \cdot \sum Q_{sp} \tag{2}$$

where Q_{ur} and Q_{gp} = load capacities of URs and GPs; η_r and η_p = P-R and R-P interaction factors; χ_g = P-P interaction factor; and Q_{sp} = load capacity of SPs. The P-P interaction factor χ_g in Eq. (2) is also referred to as the pile group effect factor and is often adopted to estimate the load capacity of GPs. The P-R and R-P interaction factors (η_r and η_p) represent changes in the load capacities of rafts and piles in comparison with those of URs and GPs.

Interaction Effect of GPs

The pile group effect caused by P-P interactions indicates differences in the load responses of SPs and GPs caused by overlapped stress and displacement fields when piles are installed in a group. Using the pile group effect factor, the load capacity of GPs can be expressed in terms of the SP load capacity as follows:

$$Q_{gp} = \chi_g \cdot \sum Q_{sp} \tag{3}$$

Both pile and soil conditions affect the values of χ_g.

According to Long (1993), χ_g can be taken as unity for medium to dense sands and higher than unity for loose sands. In practice, χ_g is often assumed as equal to 1 for conservatism (Poulos 2000). Based on the work by Castelli and Maugeri (2002), McCabe and Lehane (2006) proposed a χ_g correlation as follows:

$$\chi_g = \frac{(B_g/B_p)^{0.66}}{n} \tag{4}$$

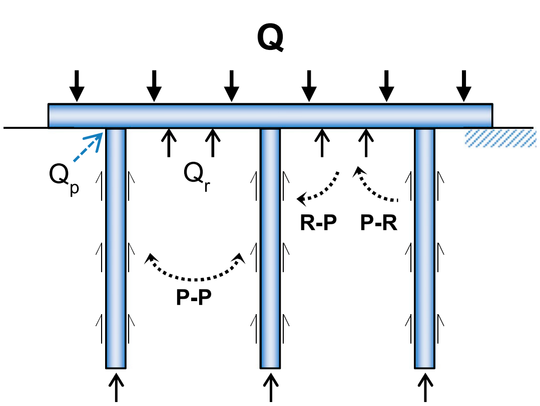

Fig. 1. Schematic view of P-P, R-P, and P-R interactions for PRs

where B_p = pile diameter; B_g = diameter of equivalent plan area of pile group; and n = number of piles. Eq. (4) indicates that the load capacity of GPs decreases as pile spacing decreases and number of piles increases.

The pile group effect is also related to the installation effect. A nondisplacement foundation such as a drilled shaft would have a much lower pile group effect than a high-displacement pile such as a closed-ended steel pipe or precast concrete pile. H-piles and open-ended steel pipes would be somewhere in between because they displace less soil. The installation of displacement piles would cause densification of the soils, with increases in horizontal stress and shaft capacity. The installation of nondisplacement piles, on the other hand, would cause stress relaxation, with decreases in shaft capacity.

Interaction Effects between Rafts and Piles

The load capacity of piles for PRs can be obtained from the load capacity of GPs considering the R-P interaction effect as follows:

$$Q_p = \eta_p \cdot Q_{gp} \tag{5}$$

The R-P interaction affects the load response of piles in two different aspects, one positive and the other negative, in regard to load-carrying capacity (Katzenbach et al. 2000). The positive effect represents increasing pile skin friction caused by increases in confining stress within the soil by raft pressure (Long 1993; Franke et al. 2000; Katzenbach et al. 2000). The effect of increasing confining stress may differ depending on stress level and location of piles within the raft. If the soil below the raft is at failure because of high raft load, plastic flow occurs and the shear stress available at the pile-soil interface may decrease. For the loads typically considered in design, however, the complete failure condition of the soil below the raft would not likely occur, and the effect of increasing confining stress would still be applicable. The negative effect, on the other hand, represents less mobilization of pile skin friction because of reduced relative displacement between piles and surrounding soils, because the soils below the raft are forced to move downward upon loading (Han and Ye 2006).

The P-R interaction represents changes in the load response of rafts caused by the load-carrying mechanism of piles. The mobilization of pile skin friction induces downward displacements of surrounding soils, which in turn leads to decreases in contact pressure between rafts and underlying soils with smaller load-carrying capacity. Introducing the P-R interaction effect, the load capacity of rafts for PRs can be written in terms of the load capacity of URs as follows:

$$Q_r = \eta_r \cdot Q_{ur} \tag{6}$$

where Q_r = load capacity of rafts for PRs.

For sandy soils, Liu et al. (1985) and Long (1993) suggested values of η_r close to unity. However, the centrifuge test results conducted by Fioravante and Giretti (2010) showed that the load capacity of rafts is smaller than that of URs, and the value of η_r is smaller than unity. This means that the use of $\eta_r = 1$ can be unconservative.

Centrifuge Tests

Test Description

A series of centrifuge tests were conducted to obtain and analyze various interaction effects of PRs embedded in sands. Four sets of centrifuge tests were conducted with two model foundations in each case using PRs, GPs, SPs, and URs. Table 1 shows detailed test conditions adopted in the centrifuge tests. The geotechnical centrifuge system used in this study had a platform radius of 5 m with a specimen chamber 900 in diameter and 700 mm in height. The centrifuge acceleration applied in the tests was $60g$, which was increased gradually for 90 min. All model foundations were manufactured considering the $1/60$ scale. More detailed specifications of the equipment and testing procedure can be found in Lee et al. (2012).

The centrifuge test specimens were prepared by the raining method using a sand diffuser system that consisted of a sand hopper and moving device. Using the sand diffuser system, the relative density (D_R) of the specimens was controlled by the fall height of sand particles, hole size, and moving speed of the sand diffuser. These were predetermined at a desired D_R through several preliminary tests. By controlling the fall height of the sand diffuser, a uniform soil layer of 1.0- to 1.5-cm thickness was formed, which was continued up to the desired ground height of 400 mm. Once the centrifuge soil specimen was formed, the weight and volume of the centrifuge chamber specimen were measured to ensure the target D_R considered in this study. The chamber space above the soil specimen was used to install loading devices and settlement measurement instrumentation.

The test soil used in the centrifuge tests was a clean silica sand with minimum and maximum dry densities ($\gamma_{d,\min}$ and $\gamma_{d,\max}$) of 12.19 and 16.12 $\mathrm{kN/m^3}$, mean particle size (D_{50}) of 0.21 mm, uniformity coefficient (C_u) of 1.96, and specific gravity (G_s) of 2.65. The values of $\gamma_{d,\max}$ and $\gamma_{d,\min}$ were determined using the vibratory table and funnel methods specified in ASTM D4253 and ASTM D4254, respectively (ASTM 2000a, b). Two D_R values of 52 and 84%, corresponding to medium and dense conditions, were adopted to prepare test specimens. Triaxial tests were conducted to further characterize the test sand for $D_R = 50$ and 80% with three confining stresses of $\sigma_3' = 50, 100$, and 200 kPa. The critical-state friction angle (ϕ_c') was 33.5°, and peak friction angles (ϕ_p') at $D_R = 50$ and 80% were 36.3° and 41.0°, respectively. These values of ϕ_p' were those averaged using the triaxial test results from the three different confining stresses.

Model Foundations

The schematic view and configurations of centrifuge tests and model foundations adopted in this study are shown in Fig. 2. The piles were made of aluminum alloy pipes with diameter of 10 and length of 250 mm. These correspond to a diameter and length of 600 mm and 15 m in prototype scale. The elastic modulus (E) of the piles was 70 GPa. The piles used in this study were all closed-ended and were driven into sand specimens under $1g$ condition after the formation of the soil specimen. Note that the horizontal stresses within the soil induced by $1g$ pile driving would be significantly lower than for piles driven under prototype conditions. The installation process in this study therefore would not represent the condition of full- or high-displacement piles, and the induced stress state could rather be close to that of nondisplacement piles in field prototype scales. The rafts were also made of aluminum and square-shaped, with width of 150 mm and thickness of 20 mm, corresponding to 9 and 1.2 m in prototype scale, respectively. Sixteen piles in a 4×4 configuration were used for GPs and PRs with pile spacing of 40 mm (2.4 m in prototype scale), corresponding to four times the pile diameter ($4B_p$).

For the installation of GPs, the pile cap was located 20 mm (1.2 m in prototype scale) above the soil surface. The embedded depth of GPs was the same as that of PRs. Four LVDTs were installed on each corner of UR, GP, and PR in order to measure settlement. Two model foundations in pair were installed within the centrifuge chamber for GP and UR, and for SP and PR. The edge-to-edge separation distances were 200 and 250 mm between GP and UR and between SP and PR. Each model foundation was loaded independently in a sequence.

Piles of PRs were instrumented to measure the loads carried by rafts and piles as well as the load transfer relationship. As shown in Fig. 2(c), six model piles were instrumented. The inner, edge, and corner piles are those instrumented. The other three piles, symmetrically placed, were instrumented to confirm the measurements. Five pairs of strain gauges were installed along the piles at depths of $0.04L$, $0.28L$, $0.52L$, $0.76L$, and $0.96L$ from the pile head. A waterproof agent (M-coat A, polyurethane coating) and epoxy resin were coated on the surfaces of the strain gauges to protect from any possible damages during installation and loading process.

Load-Settlement Curves

The load-settlement curves of UR, GP, and PR obtained from the centrifuge tests are shown in Fig. 3 for medium ($D_R = 52\%$) and dense ($D_R = 84\%$) conditions. As can be seen from Fig. 3, GP showed earlier mobilization of load-carrying capacity at smaller settlements than UR. The load-carrying capacities of GP were higher than those of UR up to settlements of 275 and 160 mm for the medium and dense cases, respectively, beyond which the load-carrying capacities of UR became reversely higher.

The load-carrying capacities of UR, GP, and PR measured at 60-mm settlement, corresponding to 10% of pile diameter ($0.1B_p$), were 15.5, 34.5, and 41.5 MN, respectively, for the medium case, and 31.0, 53.0, and 58.5 MN for the dense case. At 300-mm settlement, assumed to be close to the ultimate state, the load capacities of UR, GP, and PR were 64, 60, and 100 MN for the medium case, and 147, 102, and 182 MN for the dense case.

Predicted values of the ultimate load capacities for UR and GP were obtained using the methods described by Meyerhof (1963, 1976), with the ϕ_p' values given previously. The predicted load capacities for UR and GP [16 times SP (16SP) load capacity]

Table 1. Test Conditions for Centrifuge Tests

Test	Test name	Foundation type	Pile type	B_p (mm)	L (m)	B_r (m)	Soil condition (% D_R)
1	SP-M	SP	CEP	600	15	—	Medium (52)
	GP-M	GPs (4×4)	CEP	600	15	9	Medium (52)
2	UR-M	UR	—	—	—	9	Medium (52)
	PR-M	PR (4×4)	CEP	600	15	9	Medium (52)
3	SP-D	SP	CEP	600	15	—	Dense (84)
	GP-D	GPs (4×4)	CEP	600	15	9	Dense (84)
4	UR-D	UR	—	—	—	9	Dense (84)
	PR-D	PR (4×4)	CEP	600	15	9	Dense (84)

Note: B_r = raft width; CEP = closed-ended pile.

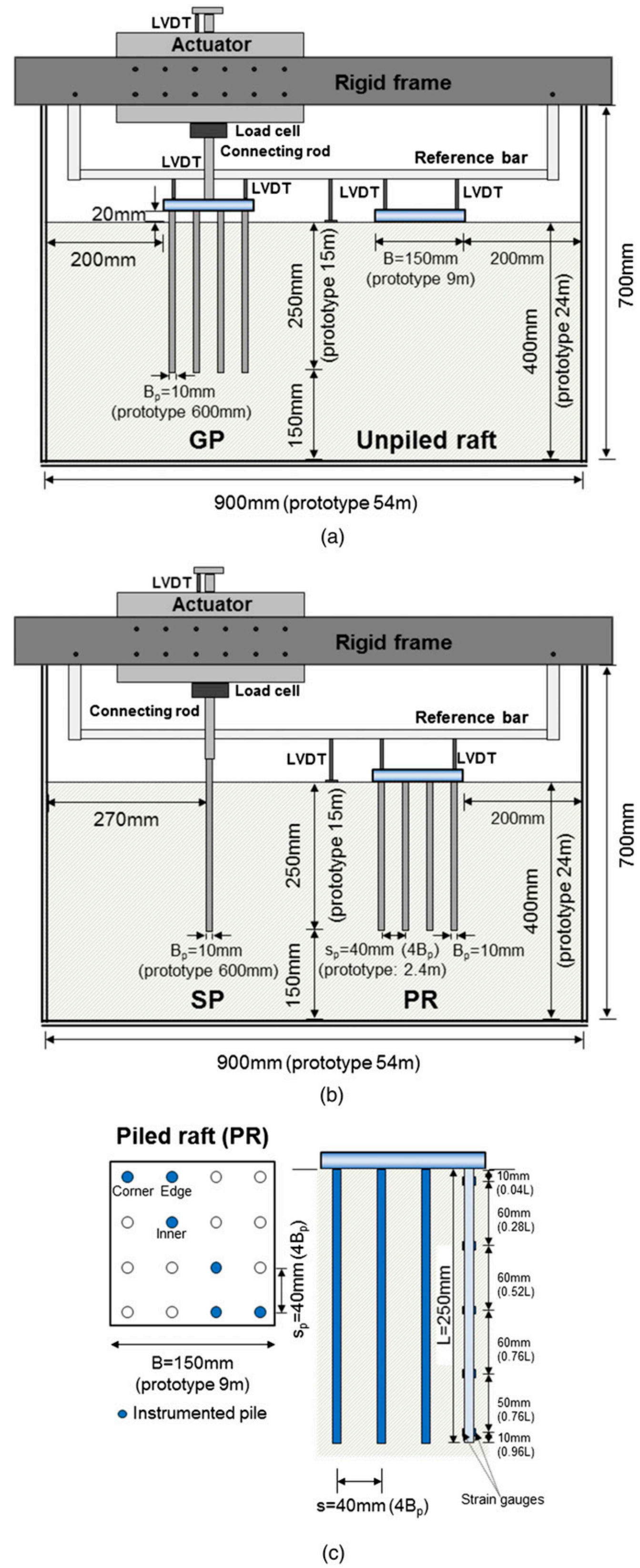

Fig. 2. Centrifuge sets of model foundations for (a) GP and UR; (b) SP and PR; and (c) configuration of instrumented piles for PR

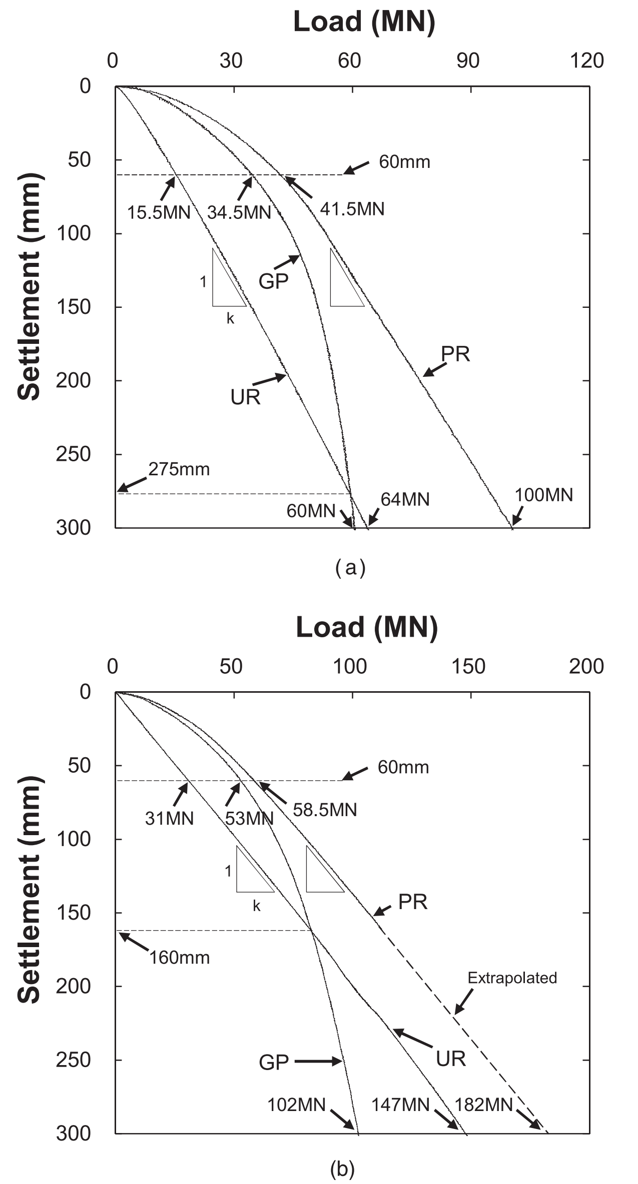

Fig. 3. Load-settlement curves of UR, GP, and PR for (a) medium ($D_R = 52\%$) and (b) dense ($D_R = 84\%$) conditions

were 175.8 and 28.5 for $D_R = 52\%$ and 494.1 and 63.8 MN for $D_R = 84\%$, respectively. For GPs, the predicted load capacities were fairly close to those measured at 60-mm settlement for both medium and dense cases. For UR, the predicted values were considerably larger (2.5–4 times) than those measured at 300-mm settlement. Such large differences indicate that the raft did not reach the fully mobilized ultimate state, because the settlement of 300 mm is in fact only 3.3% of raft width.

From Fig. 3, it is also observed that the load-settlement curves of PR are similar to those of GP initially. As load and settlement increase, the load-settlement curves of PR become similar to those of UR, showing similar load-settlement stiffness (k).

Assessment of PR Interaction Effects

Pile Group Effect

Fig. 4 shows the load-settlement curves measured from GP and calculated using 16SP load response. Those for piles of PR (P_{PR})

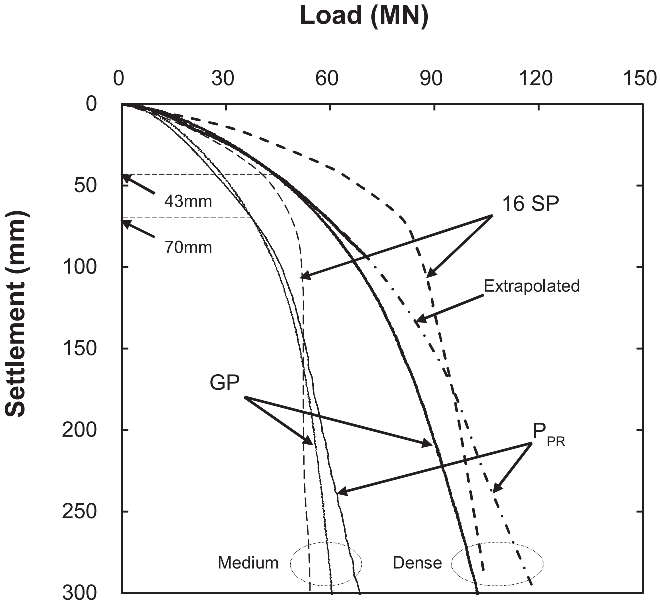

Fig. 4. Load-settlement curves of GP, P_{PR}, and 16 SP for medium and dense conditions

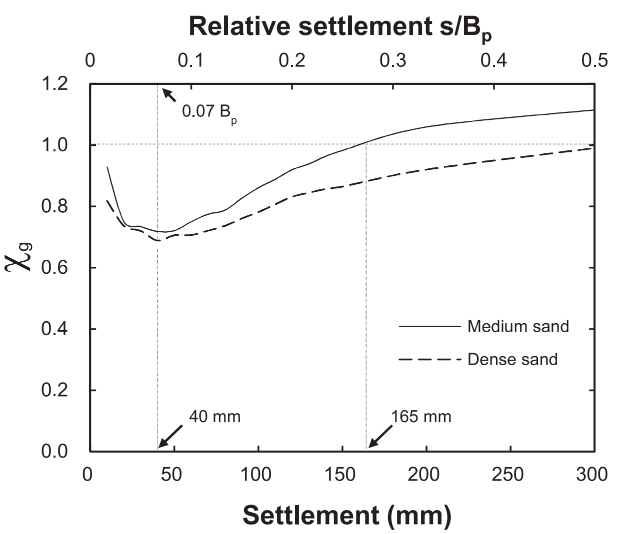

Fig. 5. Variation of χ_g values with settlement

were also included for comparison and are further analyzed later. For both cases of the medium ($D_R = 52\%$) and dense ($D_R = 84\%$) conditions, 16SP showed higher load-carrying capacities, up to settlements of 160 and 300 mm for $D_R = 52$ and 84%, respectively. Using the load-settlement curves for GPs and SPs in Fig. 4, the values of pile group effect factor χ_g were obtained and plotted in Fig. 5. The values of χ_g varied with settlement, decreasing initially and then increasing gradually with settlement, approaching certain values around unity. For the dense condition, the values of χ_g were never greater than unity up to the settlement of 300 mm. For the medium condition, χ_g became greater than unity after 165 mm of settlement. The lowest value of χ_g was approximately 0.7, observed at settlement of 40 mm ($0.07B_p$). At settlement of 300 mm, the values of χ_g were 1.11 and 0.99 for the medium and dense cases, respectively. From Figs. 4 and 5, it is seen that the primary impact of the pile-group effect represents reductions in load-settlement stiffness and load-carrying

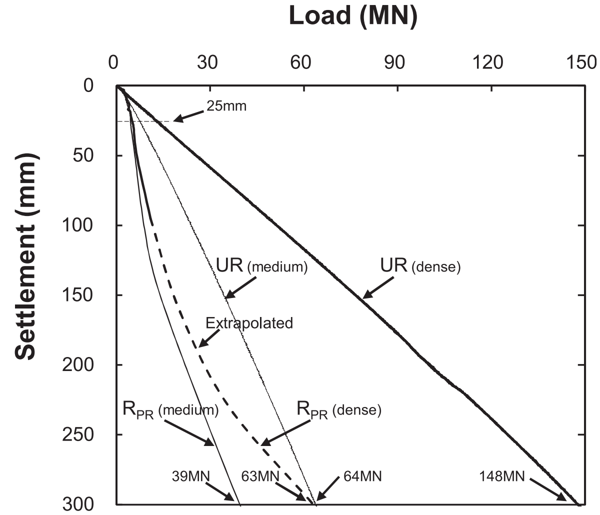

Fig. 6. Load-settlement curves of UR and R_{PR} for medium and dense conditions

capacity of piles, which become less pronounced as settlement increases.

The pile group effect observed from the centrifuge tests may differ from that for actual field scale because of differences in the size ratio of pile-to-soil particle and the effect of pile installation. It was reported that the particle size effect in centrifuge tests is not significant if the ratio of cone diameter to mean particle size (D_{50}) is greater than 20 (Gui and Bolton 1998; Balachowski 2007; Salgado 2013). The cone penetration process would be applicable to the base resistance of piles. For the centrifuge tests in this study, the ratio of pile diameter to D_{50} (B_p/D_{50}) was 50, and thus no significant particle-size effect on the base resistance was expected. For the shaft resistance, it was reported that the particle-size effect arises if B_p/D_{50} is smaller than 100 to 200 (Foray et al. 1998; Garnier and König 1998; Loukidis and Salgado 2008). This indicates that B_p/D_{50} of 50 in this study likely caused the particle-size effect on the shaft resistance, meaning that the horizontal stresses in the centrifuge tests were higher than those of prototype condition.

P-R Interaction Effect

The load-settlement curves of UR and raft of PR (R_{PR}) are shown in Fig. 6 for the medium and dense conditions. The load carried by R_{PR} was obtained by the total load imposed on PR minus the sum of axial loads measured from the individual piles. As the top strain gauges of the individual piles were installed at 1 cm (60 cm in the prototype scale) below the pile-raft connection, the friction forces within this area were not included in the load values of R_{PR}. The load-settlement curve for the dense case was extrapolated, because the strain gauges of piles were damaged after settlement of approximately 100 mm. The extrapolation was done by matching the load response of the PR and the values of η_r shown in Fig. 7. For both medium and dense cases, the load-carrying capacity of R_{PR} were lower than those of UR for the entire settlement range considered in the tests. The load-carrying capacities of R_{PR} measured at 25-mm settlement were 4.5 and 5 MN, values 40% and 59% smaller than 7.5 and 12 MN of UR for the medium and dense conditions, respectively. At 300-mm settlement level, the load capacities of R_{PR} were 39 and 63 MN, 39% and 58% smaller than 64 and 148 MN of UR for the medium and dense conditions, respectively.

Based on the load-settlement curves in Fig. 6, the values of the P-R interaction factor (η_r) were obtained and plotted in Fig. 7(a). The value of η_r decreased markedly within the initial settlement range, and then increased gradually with increasing settlement. The lowest values of η_r were 0.37 and 0.17, observed at settlements of 110 and 55 mm, corresponding to s/B_r of 0.012 and 0.006 for the medium and dense cases, respectively.

The initial decrease of η_r value can be attributed to the mobilization of pile skin friction in earlier pile loading processes, which makes the contact pressure between raft and underlying soils smaller. Once the pile skin friction was fully mobilized, the load capacity of the raft would further develop, producing higher values of η_r. It is also noticed that the initial decrease of η_r is more noticeable for the dense condition. This is because the pile load capacity in denser conditions develops at smaller settlements with stiffer load response.

Because η_r may also be affected by pile spacing, the centrifuge load test results given in Giretti (2010) for PRs with different pile spacing distances (s_p) were adopted and compared. The test results for PRs with one, three, and seven piles were adopted. For the three- and seven-pile cases, the values of s_p were 4.33 and 2.5 times the pile diameter, respectively. All tests were conducted in loose sand ($D_R \approx 30\%$). Fig. 7(b) shows the values of η_r obtained from the tests.

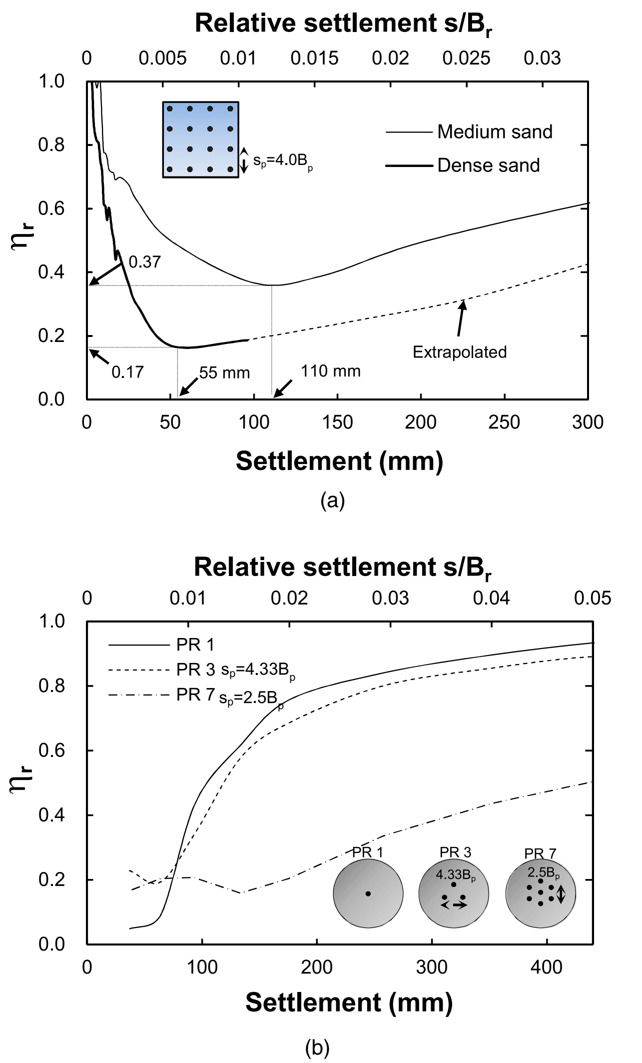

Fig. 7. Values of η_r with settlement obtained from (a) centrifuge tests in this study and (b) test results of Giretti (2010)

It is observed that the values of η_r for the seven-pile case (PR7) are smaller than for the one- and three-pile cases (PR1 and PR3). This indicates that more piles and smaller pile spacing lead to lower contact pressure between raft and underlying soils with smaller η_r.

R-P Interaction Effect

The measured load-settlement curves of GP and P_{PR} are shown and compared in Fig. 4. For both density conditions, the initial load responses of P_{PR} were similar to those of GP. After settlements of 70 and 43 mm for the medium and dense conditions, the load-carrying capacity of P_{PR} became higher than those of GP.

As discussed earlier, negative and positive effects arise from the R-P interactions. The negative effect is caused by less mobilization of pile skin friction because of downward movement of surrounding soils forced by rafts. The positive effect is caused by increasing confining stress within the soils upon loading on rafts. From Fig. 4, it is seen that the negative R-P interaction effect is not significant initially, as observed from the similar load-settlement curves of GP and P_{PR}. The positive R-P interaction effect tends to prevail with increasing settlement, showing higher load-carrying capacities of P_{PR} than of GP. The positive effect was more pronounced for the dense condition.

Using the results in Fig. 4, the values of R-P interaction factor η_p were obtained and are plotted in Fig. 8. For comparison, the values of P-R interaction factor η_r in Fig. 7 were also included. Similarly to η_r, η_p showed settlement-dependent variation. It decreased initially and then increased as settlement increased. The lowest values of η_p were 0.88 and 0.93 for the medium and dense conditions, observed at s/B_p of 0.02 and 0.025, respectively. It is observed that η_p varies much less in limited range than η_r.

Load Transfer Analysis of PRs

Load-Settlement Relationship of Individual Piles

The load responses of piles of PRs differ from those of group piles because of different load-transfer characteristics. To investigate the load-transfer mechanism of P_{PR}, the load-settlement curves of the three instrumented piles at different locations were obtained and are plotted in Fig. 9. The load-settlement curves of SP were also

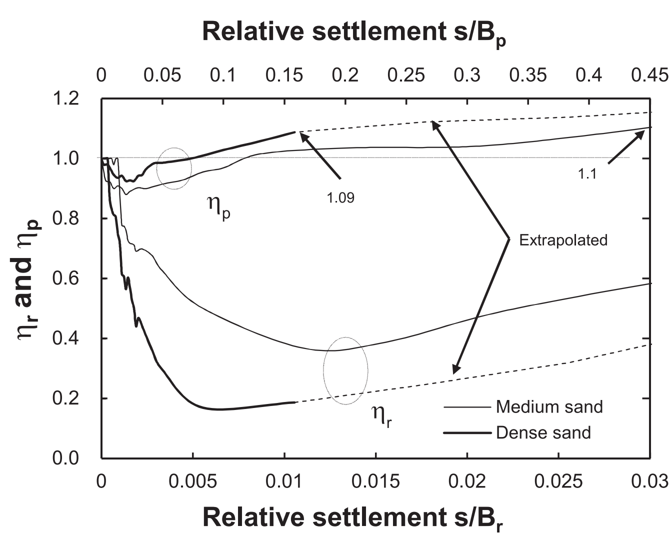

Fig. 8. Values of η_r and η_p with settlement

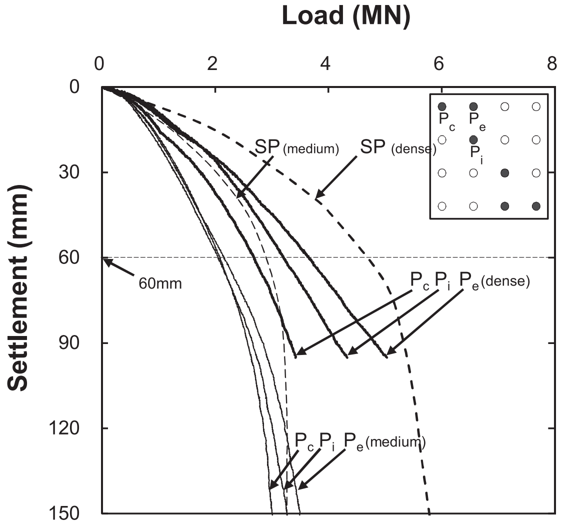

Fig. 9. Load-settlement curves of pile components for PR for medium and dense conditions

included in Fig. 9. The three piles were the inner (P_i), edge (P_e), and corner (P_c) piles as described in Fig. 2(c). For both medium and dense conditions, P_e and P_c showed the highest and lowest load-carrying capacities, respectively. All load-settlement curves of P_i, P_e, and P_c were below those of SP for settlements up to approximately 95 to 120 mm. At the settlement of 60 mm ($0.1B_p$), the load capacities of P_i, P_e, P_c, and SP were 2.1, 2.2, 2.1, and 2.9 MN for medium conditions and 3.2, 3.7, 2.7, and 4.7 MN for dense conditions.

The different load responses of P_i, P_e, and P_c can be explained based on the combined effects of pile group and R-P interaction. The pile group effect would be most significant for P_i, as it locates inside, with the largest reductions of load-settlement stiffness and load-carrying capacity. The positive R-P interaction effect with increasing confining stress, however, compensates for the negative pile group effect, which tends to produce intermediate ranges of pile load capacity. P_e, on the other hand, is subjected to lower pile group effect with less decrease in pile load capacity, whereas some increase in pile load capacity is expected because of increasing confining stress from raft pressure. As a result, P_e turned out to show the highest load-carrying capacity. The lowest load-carrying capacity of P_c can be attributed to the lowest confining stress effect.

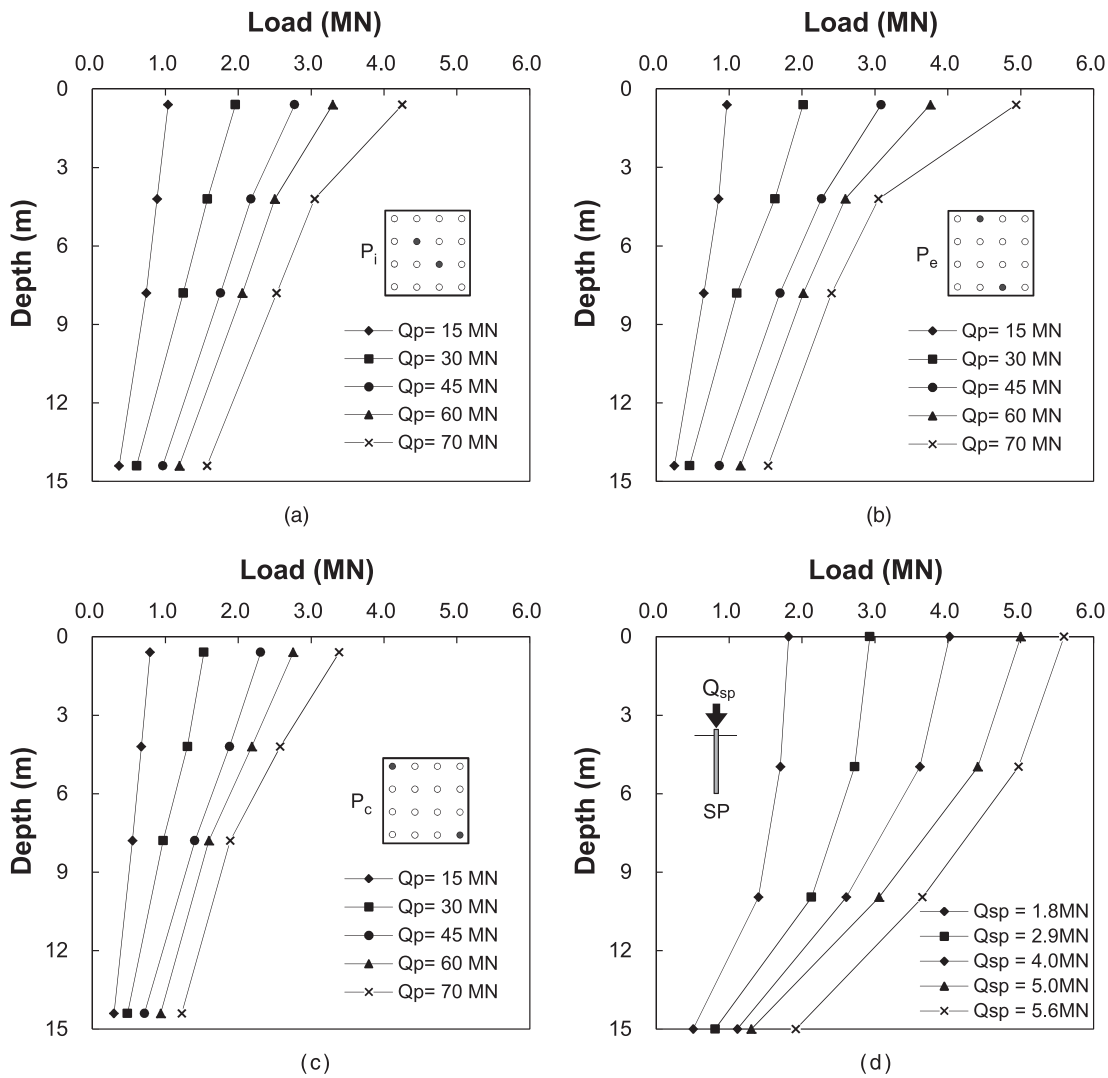

Fig. 10. Load transfer curves of (a) P_i; (b) P_e; (c) P_c; (d) SP

From Fig. 9, it is seen that the load-carrying capacities of P_i, P_e, and P_c continuously increase with settlement and become higher than that of SP at larger settlement levels. These results are comparable to the settlement-dependent variations of the pile group effect factor χ_g and R-P interaction factor η_p in Figs. 5 and 8, where the values of χ_g and η_p were smaller than unity initially and became higher than unity as settlement further increased. This indicates that the negative pile-group effect, initially observed, tends to decrease and the positive R-P interaction effect becomes predominant as settlement increases.

Load Transfer Relationship

The axial load transfer curves of P_i, P_e, and P_c were obtained and are plotted in Fig. 10 for dense sand. The results for the medium sand were similar to those for the dense case in Fig. 10. In the figures, the values of Q_p represent the loads carried by P_{PR}. The load transfer curves of SP were also included in Fig. 10. As can be identified from the pile head loads, the loads carried by P_e are larger than those by P_i and P_c, which is consistent with the results shown in Fig. 9. For $Q_p = 70$ MN, the loads carried by P_i, P_e, and P_c were 4.3, 4.9, and 3.4 MN, respectively.

The other key aspect is that the positive R-P interaction effect appears to be predominant within the upper soil zone. The pile shaft resistance was highest near the pile head and decreased along the pile. This is certainly different from the load transfer characteristics of SP given in Fig. 10(d). This can be further confirmed from Fig. 11, which shows the unit shaft capacity distributions of P_i, P_e, P_c, and SP with depth. The results in Fig. 11 were obtained by differentiating the depth distributions of axial load given in Fig. 10. For the SP in Fig. 11(d), the unit shaft capacity reached the ultimate state at $Q = 5.0$ MN, beyond which no further increase in the unit shaft capacity was observed. From the unit shaft capacities of P_i, P_e, and P_c, it is clearly seen that the R-P interaction effect produces higher pile shaft resistances within the upper soil zone. The results in Figs. 10 and 11 indicate that the positive R-P interaction effect dominates the upper soil zone, which becomes lower with increasing depth. At deeper depths, the pile group effect becomes more pronounced, producing lower unit shaft capacities.

Implications for Design Application

Using the centrifuge test results, the factors of safety (FS) of GP and PR were calculated and compared in Table 2. The values of FS in the

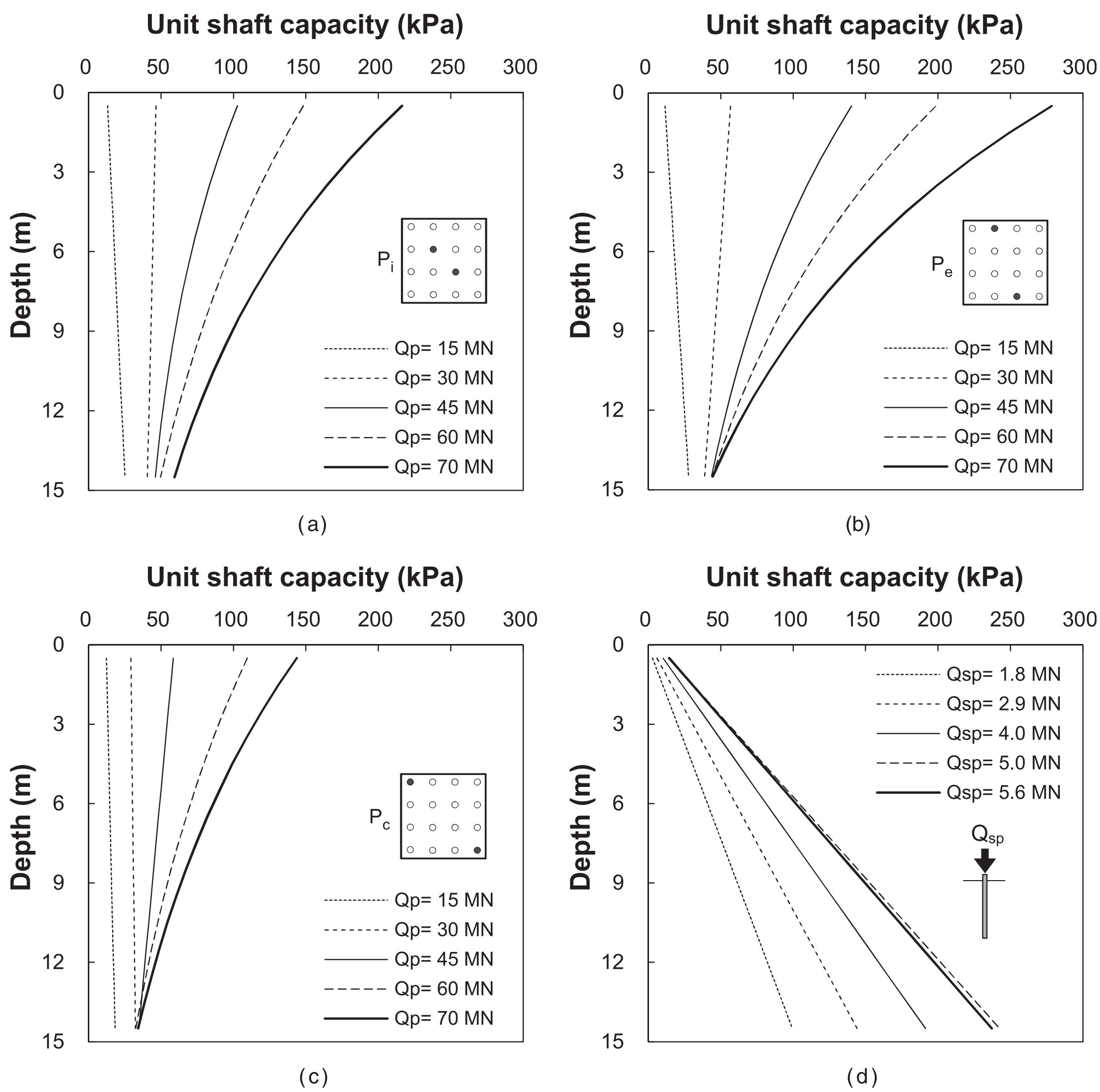

Fig. 11. Distributions of unit shaft capacity for (a) P_i; (b) P_e; (c) P_c; (d) SP

Table 2. FS for GP and PR

	FS		
Case	$s = 25$ mm	$s = 60$ mm	Soil condition (% D_R)
GP-M	2.81	1.73	Medium (52)
PR-M	4.65	2.86	Medium (52)
GP-D	3.33	1.62	Dense (84)
PR-D	5.95	2.89	Dense (84)

table were obtained for loads applied to GP at settlements of 25 and 60 mm ($0.1B_p$) with the ultimate load capacities of GP and PR (i.e., $Q_{gp,\mathrm{ult}}$ and $Q_{pr,\mathrm{ult}}$). The FS for GP varied from 1.62 to 3.33, indicating that additional piles may be necessary considering the typical FS of 3. With the contribution of rafts as designed as PR, FS increased to the 2.86–5.95 range.

The FS of PRs can be evaluated in terms of those of URs and GPs given as follows (de Sanctis and Mandolini 2006):

$$\mathrm{FS}_{pr} = \zeta_{pr}\left(\mathrm{FS}_{ur} + \mathrm{FS}_{gp}\right) \tag{7}$$

where FS_{pr}, FS_{ur}, and FS_{gp} = FS for PRs, URs, and GPs; and ζ_{pr} = load capacity efficiency factor = $Q_{pr}/(Q_{ur} + Q_{gp})$. The values of ζ_{pr} obtained from the centrifuge tests are shown in Fig. 12(a) in comparison with η_p and η_r described previously. It is seen that ζ_{pr} decreases gradually with settlement and converges on 0.80 and 0.73 for the medium and dense cases, respectively. This range of ζ_{pr} values is lower than for clays reported in de Sanctis and Mandolini (2006), indicating that a higher interaction effect occurs in sands with more changes (less efficiency) in the load-carrying capacities of rafts and piles.

As different levels of tolerable settlement are considered in the performance-based design, such as the LRFD and limit state design, the values of ζ_{pr}, η_p, and η_r at different settlements were obtained and are shown in Table 3 for settlements of 25, 60, and 200 mm. The 25-mm settlement represents the typical settlement level corresponding to the serviceability limit state, whereas the other two may correspond to those for the ultimate limit state at larger settlement levels.

Because of the changes in raft and pile load capacities with various interaction effects, the mobilized FS for R_{PR} and P_{PR} would be different from that of PR. Using the decomposed load-settlement curves of R_{PR} and P_{PR} in Figs. 4 and 6, the mobilized factors of safety FS_r, FS_p, and FS_{pr} for R_{PR}, P_{PR}, and PR were obtained and are plotted in Fig. 12(b) for the medium condition. The results for the dense condition were similar to those in Fig. 12(b). The loads used to calculate FS_r and FS_p in Fig. 12 were those carried by R_{PR} and P_{PR} for a given load imposed on PR. The ultimate load capacities of R_{PR} and P_{PR} were also determined from the decomposed load-settlement curves. It is seen that FS_r of rafts is always higher than FS_p and FS_{pr} of piles and PRs. The higher FS_r implies that less load is transmitted to rafts, which was particularly true within the initial loading range. As settlement increases, the difference becomes smaller and all FS values of rafts, piles, and PRs eventually reach failure with FS = 1. This indicates that the interaction effects alter the mobilization of raft load-carrying capacity, and the load sharing behavior between rafts and piles should properly be considered for the design of PRs.

Summary and Conclusions

As PRs represent a combined structural system of different foundation components, interaction effects arise and affect the overall load responses of PRs. In the current study, the load responses and interaction effects of PRs embedded in sands were investigated. A series of centrifuge load tests were conducted using different types of model foundations. URs and PRs, and SPs and GPs were adopted in the tests to analyze various interaction effects of PRs in sands.

The load-settlement curves of PRs were similar to those of GPs in the earlier loading stage and became similar to those of URs with similar load-settlement stiffness. The PR interaction effect factors investigated in this study all showed settlement-dependent variations. The pile-group effect factor decreased initially and increased gradually with increasing settlement, approaching certain values

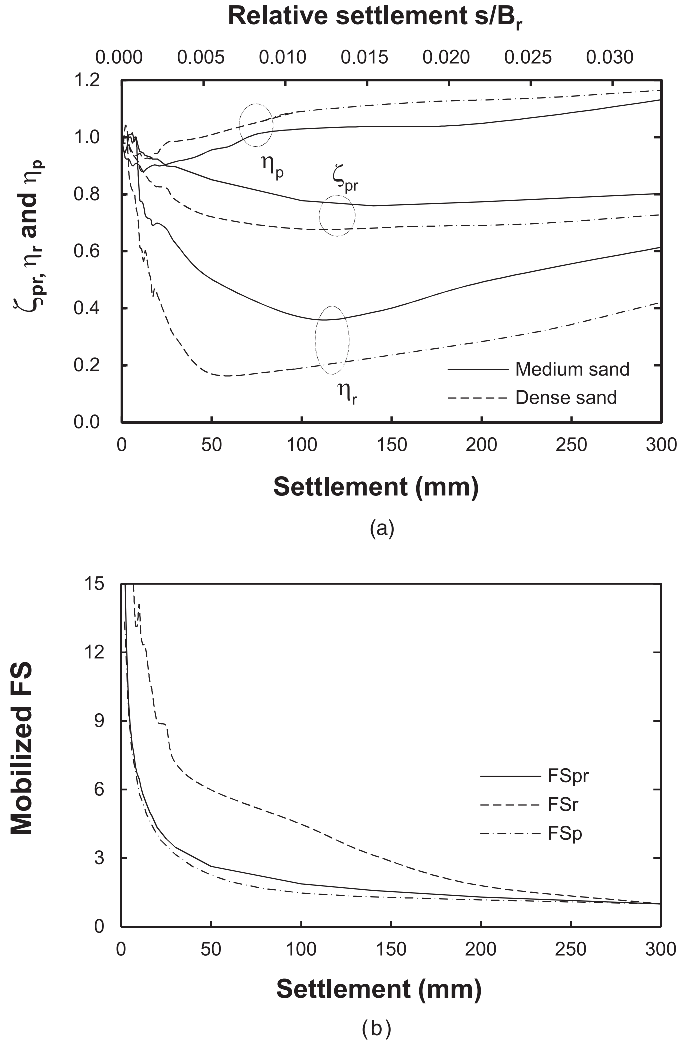

Fig. 12. Variation of interaction parameters and mobilized FS: (a) values of ζ_{pr}, η_r, and η_p and (b) mobilized FS with settlement

Table 3. Values of ζ_{pr}, η_p, and η_r for Different Settlement Levels

	$s = 25$ mm		$s = 60$ mm		$s = 200$ mm	
Factor	$D_R = 52\%$	$D_R = 84\%$	$D_R = 52\%$	$D_R = 84\%$	$D_R = 52\%$	$D_R = 84\%$
ζ_{pr}	0.90	0.80	0.83	0.70	0.78	0.70
η_p	0.90	0.98	0.98	1.02	1.04	1.12
η_r	0.66	0.35	0.49	0.18	0.50	0.30

around unity. Both P-R and R-P interaction factors decreased within the initial settlement range and increased with increasing settlement. The initial reduction of the P-R interaction factor was caused by the mobilization of pile skin friction that developed earlier in the pile loading process, which made the contact pressure between rafts and underlying soils smaller. The range of the P-R interaction factor was much larger than that of the R-P interaction factor.

The load response and load-transfer relationship of piles for PRs were different from those of SPs. The edge piles showed the largest load-carrying capacity, and the R-P interaction effect was predominant within the upper soil zone. The mobilized FS for rafts was always higher than of piles and PRs because of less transmission of load to rafts.

Acknowledgments

This work was supported by Basic Science Research Program through the National Research Foundation of Korea (NRF) grants funded by the Korean government (MSIP) (Nos. 2011-0030040 and 2013R1A1A2058863).

References

ASTM. (2000a). "Standard test methods for maximum index density and unit weight of soils using vibratory table." *D4253*, West Conshohocken, PA.

ASTM. (2000b). "Standard test methods for minimum index density and unit weight of soils and calculation of relative density." *D4254*, West Conshohocken, PA.

Balachowski, L. (2007). "Size effect in centrifuge cone penetration tests." *Arch. Hydro-Eng. Environ. Mech.*, 54(3), 161–181.

Burland, J. B. (1995). "Piles as settlement reducers." *Proc., 19th Italian National Geotechnical Congress*, SF Editoriali, Padova, Italy, 2, 21–34.

Castelli, F., and Maugeri, M. (2002). "Simplified nonlinear analysis for settlement prediction of pile groups." *J. Geotech. Geoenviron. Eng.*, 10.1061/(ASCE)1090-0241(2002)128:1(76), 76–84.

Conte, G., Mandolini, A., and Randolph, M. F. (2003). "Centrifuge modelling to investigate the performance of piled rafts." *Proc., 4th Int. Geotechnical Seminar on Deep Foundations on Bored and Auger Piles*, W. F. Van Impe, ed., Millpress, Rotterdam, Netherlands, 359–366.

Davis, E. H., and Poulos, H. G. (1972). "The analysis of piled raft systems." *Aust. Geotech. J.*, G2(1), 21–27.

de Sanctis, L., and Mandolini, A. (2006). "Bearing capacity of piled rafts on soft clay soils." *J. Geotech. Geoenviron. Eng.*, 10.1061/(ASCE)1090-0241(2006)132:12(1600), 1600–1610.

Fioravante, V., and Giretti, D. (2010). "Contact versus noncontact piled raft foundations." *Can. Geotech. J.*, 47(11), 1271–1287.

Foray, P., Balachowski, L., and Rault, G. (1998). "Scale effect in shaft friction due to the localisation of deformations." *Proc., Centrifuge 98*, Taylor & Francis, Oxford, U.K., 211–216.

Franke, E., El-Mossallamy, Y., and Wittmann, P. (2000). "Calculation methods for raft foundations in Germany." *Design applications of raft foundations*, J. A. Hemsley, ed., Thomas Telford, London, 282–322.

Garnier, J., and König, D. (1998). "Scale effects in piles and nails loading tests in sand." *Proc., Centrifuge 98*, Taylor & Francis, Oxford, U.K., 205–210.

Giretti, D. (2010). "Modelling of piled raft foundations in sand." Ph.D. thesis, Univ. of Ferrara, Ferrara, Italy.

Gui, M. W., and Bolton, M. D. (1998). "Geometry and scale effects in CPT and pile design." *Proc., Geotechnical Site Characterization*, Balkema, Rotterdam, Netherlands, 1063–1068.

Han, J., and Ye, S.-L. (2006). "A field study on the behavior of a foundation underpinned by micropiles." *Can. Geotech. J.*, 43(1), 30–42.

Horikoshi, K., and Randolph, M. F. (1996). "Centrifuge modelling of piled raft foundations on clay." *Géotechnique*, 46(4), 741–752.

Horikoshi, K., and Randolph, M. F. (1998). "A contribution to the optimum design of piled rafts." *Géotechnique*, 48(3), 301–317.

Katzenbach, R., Arslan, U., and Moormann, C. (2000). "Piled raft foundation projects in Germany." *Design applications of raft foundations*, J. A. Hemsley, ed., Thomas Telford, London, 323–391.

Lee, J., Park, D., Kyung, D., Choi, K., and Choi, Y. (2012). "The optimization of bridge foundation design." *Rep. No. RKO 2012-013*, Korea Institute of Construction Technology, Goyang, Korea.

Liu, J. L., Yuan, Z. L., and Shang, K. P. (1985). "Cap-pile-soil interaction of bored pile groups." *Proc., 11th Int. Conf. on Soil Mechanics and Foundation Engineering (ICSMFE)*, Balkema, Rotterdam, Netherlands, 3, 1433–1436.

Long, P. D. (1993). "Footings with settlement-reducing piles in noncohesive soil." Ph.D. thesis, Chalmers Univ. of Technology, Gothenburg, Sweden.

Loukidis, D., and Salgado, R. (2008). "Analysis of the shaft resistance of non-displacement piles in sand." *Géotechnique*, 58(4), 283–296.

McCabe, B. A., and Lehane, B. M. (2006). "Behavior of axially loaded pile groups driven in clayey silt." *J. Geotech. Geoenviron. Eng.*, 10.1061/(ASCE)1090-0241(2006)132:3(401), 401–410.

Meyerhof, G. G. (1963). "Some recent research on the bearing capacity of foundations." *Can. Geotech. J.*, 1(1), 16–26.

Meyerhof, G. G. (1976). "Bearing capacity and settlement of pile foundations." *J. Geotech. Engrg. Div.*, 102(GT3), 195–228.

Poulos, H. G. (2000). "Practical design procedures for piled raft foundations." *Design applications of raft foundations*, J. A. Hemsley, ed., Thomas Telford, London, 425–467.

Reul, O., and Randolph, M. F. (2003). "Piled rafts in overconsolidated clay: Comparison of in situ measurements and numerical analyses." *Géotechnique*, 53(3), 301–315.

Salgado, R. (2013). "The mechanics of cone penetration: Contribution from experimental and theoretical studies." *Geotechnical and Geophysical Site Characterization 4*, CRC Press, Boca Raton, FL, 131–153.